SCIENCE CHINA
Chemistry

• ARTICLES •

April 2013 Vol.56 No.4: 514–523
doi: 10.1007/s11426-012-4802-8

A molecular dynamics and computational study of human KAT3 involved in KYN pathway

XU Yu, ZHENG QingChuan*, YU LiYing, ZHANG HongXing* & SUN ChiaChung

State Key Laboratory of Theoretical and Computational Chemistry, Institute of Theoretical Chemistry, Jilin University, Changchun 130023, China

Received August 3, 2012; accepted August 20, 2012; published online December 31, 2012

Kynurenine aminotransferases (KATs) catalyze the transamination of kynurenine (KYN) pathway and endogenous KYNs have been suggested to highly correlate to abnormal brain diseases. HKAT3 is a key member of KAT family, while the binding mechanism of KYN and cofactor with HKAT3 has not been determined yet. In this study, we focus on the structure-function relationship among KYN, cofactor and HKAT3. The binding models of KYN complex and KYN&cofactor complex were obtained and were studied by molecular dynamics (MD) simulations. We identified several critical residues and influence of conformational changes in human kynurenine aminotransferase 3 (HKAT3) complexes. The cofactor may contribute largely not only to the catalysis, but also to the binding. In addition, a hypothesis is proposed that a strong hydrophobic interaction between Tyr159 and Lys280 may influence the binding mode and the binding region of the substrate and the cofactor. Our results will be a good starting point for further determination of the biological role.

kynurenine (KYN), kynurenine aminotransferases (KATs), π-π interaction, molecular dynamic (MD) simulation, interaction energy

1 Introduction

Kynurenic acid (KYNA), which is the key intermediate in the KYN pathway, is produced enzymatically by irreversible transamination of kynurenine (KYN). It has been reported that KYNA can function as an antagonist of the α7-nicotinic acetylcholine receptor in cultured hippocampal neurons and an endogenous ligand of the orphan G protein-coupled receptor (GPR35) [1–4]. Moreover, KYNA is the only known endogenous antagonist of *N*-methyl-*D*-aspartate (NMDA) subtype of glutamate receptors [5–9]. These results suggest that endogenous KYNs may participate in normal brain function as modulators of glutamatergic neurotransmission. In particular, multiple neurodegenerative diseases, such as Huntington disease, Alzheimer's disease, Schizophrenia, and Acquired immunodeficiency syndrome dementia, have been suggested to correlate to abnormal KYNA levels in the central nervous system [10–16].

Kynurenine aminotransferases (KATs), members of the aminotransferase family, catalyze the transamination of KYN into KYNA utilizing a vitamin B6 derivative (pyridoxamine 5-phosphate, PMP) as cofactor. Four proteins (KAT I, KAT II, KAT III, and KAT IV) have been considered to be involved in KYNA synthesis in the central nervous system of humans, rats, and mice [17–23]. KAT II and KAT IV, which are considered to be the mitochondrial proteins, are phylogenetically distant from KAT I and KAT III [24–35]. However, KAT I and KAT III share the highest sequence identity, particularly with an identity of 51.7% in humans.

Since the first crystal of KAT family was determined at 2.0 Å in 2004 [36], thirty-one structure hits, with or without substrates at all levels of resolution, have been found. In a previous study, we have built the homology model of hu-

*Corresponding authors (email: zhengqc@jlu.edu.cn; zhanghx@jlu.edu.cn)

man KAT III (HKAT3) successfully, and have studied the binding modes of its inhibitors (*L*-methionine and *L*-tryptophan) [37]. However, the binding mechanism of KYN with HKAT3 and the influence of cofactor have not been determined yet. A detailed understanding of the catalytic action of HKAT3 requires an accurate 3D structure of the complexes for exploring the structure-function relationship.

In this study, the transamination mechanism of KYN, catalyzed by HKAT3, is theoretically determined by performing molecular dynamic (MD) simulation. The molecular binding modes have been adopted to determine the structures of biomolecular complexes and compare the influence of PMP. We reveal the mechanism of interactions among KYN, PMP and HKAT3. The results are instrumental to exploration of the catalytic properties of this enzyme as well as the interactions of this protein with the substrate and the intermediates along the reaction path. Furthermore, the finding will lead to the final product KYNA and might be a good starting point for further determination of the biological role.

2 Methods

We built the model of HKAT3 complexes, based on the published model [37] which includes chain A and chain B (see details in online Supplement). The complex models were subjected to MD simulation. The average structure during MD simulation was calculated and evaluated.

2.1 Inhibitor binding study

The KAT members share similar binding sites. The inhibitors, including KYN and KYN&PMP (see details in online Supplement), were put into the binding pocket with the coordinate extracted directly from the complex of KAT family (PDB: 3E2Z) [23].

2.2 Molecular dynamics (MD) simulations

The initial structures of HKAT3, HKAT3-KYN complex and HKAT3-KYN&PMP complex were taken for individual 5 ns MD simulation calculations. GROMACS v4.0.5 [38] was used to conduct the simulation with the GROMOS96 53a6 force field [39] on a high performance Linux cluster computer. The topology files and charges for the ligand atoms were calculated using the PRODRG web-server [40]. Each model was inserted into a water box of 0.9 nm from the surface of the protein. The systems were neutralized with 2 Cl^- ions in each system and the number of Na^+ ions was 10, 3 and 11 (in HKAT3, HKAT3-KYN complex, HKAT3-KYN&PMP complex system), respectively. The energy minimization was performed using steepest descent (SD) for 5000 steps. The total numbers of the atoms in each system are 67864, 83200 and 83423 (HKAT3, HKAT3-KYN complex and HKAT3-KYN&PMP complex system, respectively). The value of pH was set to 7 according to the pH value in a previous experimental study [22]. Then individual protein backbones were frozen and the ligands and solvent molecules with counter-ions were allowed to move during a 300 ps position restrained (1000 kJ mol nm^{-2}) MD run. Finally, a 5 ns production run was performed in each system with the simulation period, chosen as a compromise between the quality of configuration space sampling and the calculation length. The electrostatic interactions were calculated by the particle mesh Ewald (PME) algorithm [41, 42], with an interpolation order of 4 and a grid spacing of 0.12 nm. All simulations were run under periodic boundary conditions with NPT ensemble using Berendsen's coupling algorithm to keep the temperature at 300 K and the pressure (1 bar) constant with isotropic molecule-based scaling. Bond lengths were constrained with the LINCS algorithm [43], which made it possible to extend time steps to 2 fs. The coordinates were stored for every 10 ps for analysis. The van der Waals (vdW) forces were treated by a cutoff of 12 Å. VMD and Chimera were used for visualization [44, 45].

2.3 Analysis of molecular dynamic simulation

The analyses of the trajectory, including the calculation of root mean square deviations (RMSD) and average interaction energy, were performed by GROMACS 4.5.3. Systems were well equilibrated and stabilized after the first 1 ns simulations according to RMSD of all protein C_α atoms. The trajectories of each system were involved in the interaction network analysis. The Simulaid program [46] was used to calculate the hydrogen-bonding interactions and hydrophobic contacts, which are important in binding with ligands [47]. The Simulaid outputs for interactions were reorganized with in-house scripts for the facility of comparison among the systems.

3 Results

3.1 Stability of HKAT3 complex structures during MD simulations

To gain further insight into the substrate-binding mechanism in HKAT3, time-dependent atomic motions were explored by MD simulations. In order to compare the protein structures from the three different systems, their representative structures were selected from each 5 ns MD simulation. The average structures of these systems were calculated, and their regions of binding sites are shown with surface in Figure 1. The C_α RMSD values of each system (single HKAT3, KYN-HKAT3 complex and KYN&PMP-HKAT3 complex) during the last 1 ns are 0.30, 0.33 and 0.19 nm, respectively (Figure 2). In addition, based on the calculation

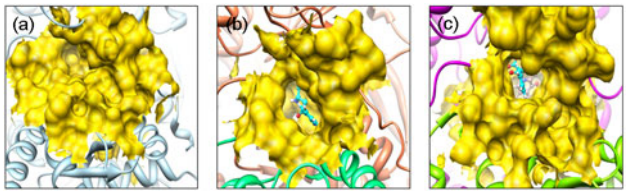

Figure 1 Average structures of three systems at the end of 5 ns MD run. (a) The system of HKAT3 alone: ribbons are in light blue and surface is in gold; (b) the system of HKAT3&KYN complex: chain A is in salmon, chain B is in spring green, surface is in gold and the ligand is shown in ball & stick; (c) the system of HKAT3&KYN&PMP complex: chain A is in magenta, chain B is in chartreuse, surface is in gold and the ligands are shown in ball & stick.

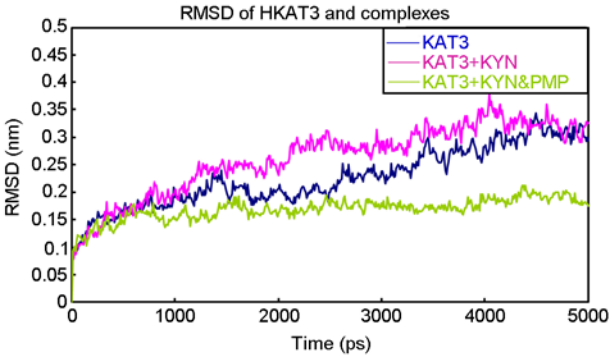

Figure 2 The C_α RMSD of HKAT3 and its complexes during 5 ns MD simulation, including HKAT3 alone (colored in dark blue), HKAT3&KYN complex (colored in magenta), and HKAT3&KYN&PMP complex (colored in green). All of the three systems stabilized around 1.5–3.5 Å at the last 1 ns, respectively.

of GROMACS program, the interaction energy (the short range electrostatic interaction energy) between each of the ligands (KYN and KYN&PMP) and HKAT3 is −7.66 and −14.64 kJ/mol. These results indicate that the KYN&PMP-HKAT3 complex system is more stable than the KYN-HKAT3 complex system.

3.2 MD simulation of the KYN-HKAT3 complex (KYN complex)

In the initial structure used as the starting point for the production run, the KYN binds in a hydrophobic pocket and its benzyl ring forms π-π interaction with the indole side chains of Trp53. As shown in Figure 3(a), the amino moiety of KYN forms hydrogen bond mainly with Tyr159. Moreover, the benzyl part of Phe372 is involved in hydrophobic interaction with carboxyl part of the ligand. This binding mode is in good agreement with the site-directed mutagenesis investigation on mouse KAT3 and the other members of KAT family [1]. During the first 3 ns, Try311(B) moves towards the substrate, thus KYN is sandwiched by Trp53 and Try311(B) *via* π-π interaction (Figure 3(b)). Meanwhile, N_{H1} atom of Arg429 forms a salt-bridge with the carboxyl group of the ligand. In the last 2 ns MD simulation, Try97(B), which acts as an anchor, participates in hydrophobic interaction with KYN and keeps their distance about 4.0 Å (Figure 3(c)). In addition, our data indicate that Gln70 and Gln307(B) interact hydrophobically with the ligand molecule (Table 1).

3.3 MD simulation of the KYN&PMP-HKAT3 complex (KYN&PMP complex)

Previous investigations revealed that the PMP, acting as a cofactor, is necessary for the protein's biological activity and is able to stabilize the binding of ligands in the active

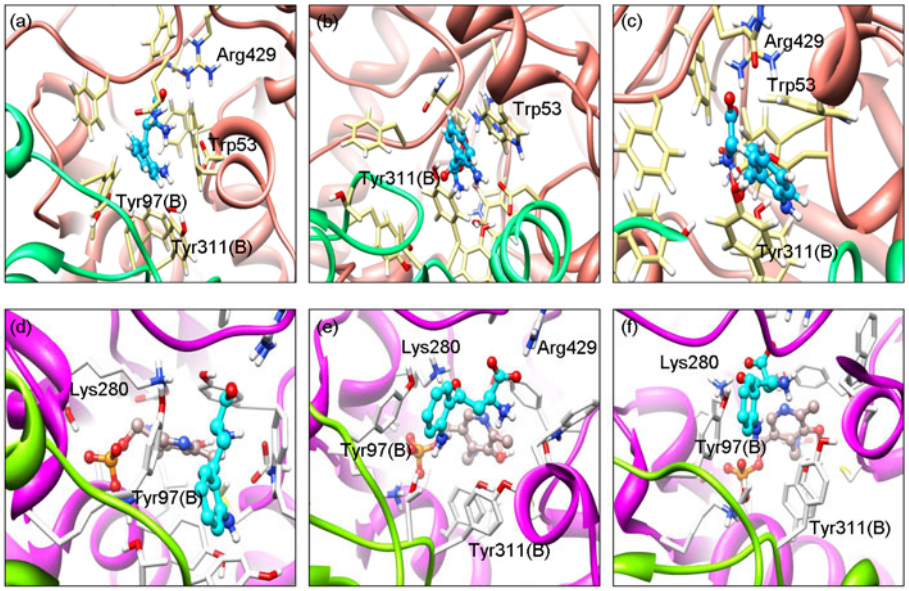

Figure 3 Snapshots of the complex systems during 5 ns MD run. The system of HKAT3&KYN complex: chain A is in salmon, chain B is in spring green and the ligand is shown in ball & stick. (a) At 0 ns; (b) at 2.5 ns; (c) at 5 ns. The system of HKAT3&KYN&PMP complex: chain A is in magenta, chain B is in chartreuse and the ligands are shown in ball & stick. (d) At 0 ns; (e) at 2.5 ns; (f) at 5 ns.

Table 1 The fraction of hydrophobic interaction during 5 ns MD simulation in each of the two complexes (Unit: 1)

H KAT3			KYN-alone	KYN&PMP	
ResName	Resid	Chain		PMP	KYN
Thr	312	B	0.17	0	0.52
Tyr	311	B	0.57	0.05	0.22
Asn	308	B	0.1	0	0
Gln	307	B	0.37	0	0
Gly	100	B	0	0	0.05
Arg	99	B	0	0	0.05
Thr	98	B	0.01	0	0.09
Tyr	97	B	0.13	0.05	0.64
Arg	429	A	0.06	0	0.87
Phe	415	A	0	0.16	0.25
Phe	372	A	0.25	0	0.48
Tyr	371	A	0.09	0	0.02
Lys	288	A	0	0.02	0.01
Thr	285	A	0.01	0	0
Lys	280	A	0.06	0.7	0.45
Gly	279	A	0	0.01	0
Ser	277	A	0	0.01	0
Ile	275	A	0	0.21	0
Tyr	249	A	0	0.21	0
Val	248	A	0	0.73	0
Asp	246	A	0	0.05	0
Met	165	A	0	0.1	0
Tyr	162	A	0	0.1	0
Cys	161	A	0.02	0.53	0
Asp	160	A	0.31	0.46	0
Tyr	159	A	0.34	0.71	0.52
Leu	138	A	0	0.41	0
Tyr	135	A	0.16	0.63	0.02
Ala	134	A	0	0.79	0
Pro	73	A	0.03	0	0.02
Phe	72	A	0.07	0	0.41
Gly	71	A	0.3	0	0.65
Gln	70	A	0.31	0	0.67
Thr	57	A	0.14	0	0.02
Ile	54	A	0.05	0	0

site [1]. Our MD simulation results of the KYN&PMP complex show that the position of ligands does not change much during the entire 5 ns MD simulation. Try97(B), which acts as an anchor, participates in π-π interaction with the KYN moiety along MD run (Figure 3(d), (e) and (f)). Gln70 and Phe72 are involved in hydrophobic interactions with aromatic moiety of the KYN. Meanwhile, the salt-bridge between Arg429 and the carboxyl group of the KYN is also found in the presence of PMP. As to PMP, the phosphate group forms hydrogen bond mainly with Lys288 and Ser277 (Table 2). It is noteworthy that the key residue Asp246 forms a salt-bridge with the N_4 atom of PMP during the MD simulation, which is believed to be an important feature of binding to PMP [1]. Meanwhile, an important hydrophobic network, involving Tyr159, Lys280 and both of the ligands (KYN and PMP), is found during the MD simulation. This network contributes largely to fixing the relative positions of the cofactor and KYN. Additionally, the benzyl moiety of PMP lies inside the hydrophobic region (including Tyr135, Cys161, and Tyr162), which is also identified in the complexes of KAT family by experimental studies [1].

4 Discussion

4.1 Conformational changes during the process of ligand binding

Figure 1 shows the secondary structure changes of the binding sites in all the three systems. The binding pocket stays open ($Distance_{Tyr159\text{-}Lys280} > 0.6$ nm) to allow ligands moving towards the active site (Figure 1(a)), and becomes closed ($Distance_{Tyr159\text{-}Lys280} < 0.4$ nm) with substrates (Figure 1(b) and (c)).

Table 2 The fraction of hydrogen bonds during 5 ns MD simulation in each of the two complexes (Unit: 1)

H KAT3			KYN-alone	KYN&PMP	
ResName	Resid	Chain		PMP	KYN
Thr	312	B	0.01	0.1	0.31
Tyr	311	B	0.12	0	0.2
Asn	308	B	0.02	0	0
Gln	307	B	0.16	0	0
Gly	100	B	0	0	0.01
Arg	99	B	0	0	0.04
Tyr	97	B	0.04	0.09	0.13
Arg	429	A	0.19	0	0.73
Phe	415	A	0	0	0.11
Phe	372	A	0.33	0	0.37
Tyr	371	A	0.12	0	0.03
Lys	288	A	0	0.23	0
Lys	280	A	0.03	0.07	0.12
Gly	279	A	0	0.01	0
Ser	277	A	0	0.5	0
Tyr	249	A	0	0.46	0.01
Asp	246	A	0	0.38	0
Asn	218	A	0.09	0	0
Asn	214	A	0	0.01	0
Tyr	162	A	0	0.08	0
Cys	161	A	0.01	0.15	0
Asp	160	A	0.3	0	0.18
Tyr	159	A	0.23	0.16	0.25
Tyr	135	A	0.22	0.45	0.02
Ala	134	A	0	0.46	0
Phe	72	A	0.03	0	0.17
Gly	71	A	0.23	0	0.43
Gln	70	A	0.24	0	0.05
Trp	53	A	0.11	0	0.07

The large change between the structure in single HKAT3 and that in two HKAT3 complexes can be found apparently in the C_α RMSD curves (Figure 2). The two HKAT3 complexes simulations reach equilibration after about 2.5 ns from the beginning. The RMSD value of KYN&PMP complex is stabilized near 0.19 nm, lower than KYN complex (0.33 nm), while RMSD values of the single HKAT3 system increase in the first 4.5 ns, and become stable around 0.30 nm in the last 0.5 ns. These results demonstrate that the HKAT3 protein in the presence of KYN&PMP is the most stable in the three systems.

The root-mean-square fluctuations (RMSF), an important indicator for comparing the structures of biomolecules, were examined for the C_α atoms of each residue. We compared the fluctuations of the protein in the three systems during the MD simulations (Figure 4). The atomic fluctuations of the binding region in single HKAT3 are slightly higher than those in HKAT3 complexes, suggesting that average RMSF values are decreased by the binding of ligands. These decreases in values indicate that KYN and PMP influence the enzymatic activity of HKAT3. For example, the RMSF of the first α-helix along the *N*-terminal (chain A: aa52-64), where a shift has been reported to exist upon binding of ligands [1], decreases by the interaction with ligands. The distance between the benzyl ring C_Z atom of KYN and the C_{D2} atom of aromatic side chain group of Trp53 was changed from 5.93 Å to 4.08 Å. We conjecture that this conformational change might be an influencing factor of the active pocket closing.

The results mentioned above demonstrate that the binding of ligands disrupts the tertiary structure of HKAT3, rather than the secondary structure inside the binding pocket. The conformational changes of HKAT3 may allow the recognition of ligands and will plug the active center after binding.

4.2 Role of interactions between Tyr159 and Lys280

In both complexes, the aromatic rings of the KYN form π-π interaction with aromatic side chains of Tyr159. Previous studies showed that this residue plays important roles both in catalysis and in binding [48]. In this study, an interesting hydrophobic interaction is found between Tyr159 and Lys280 in HKAT3 complexes. In addition, the distances between the O_H atom of Tyr159 and the C_Z atom of Lys280 were monitored to study the relationship between the pro-

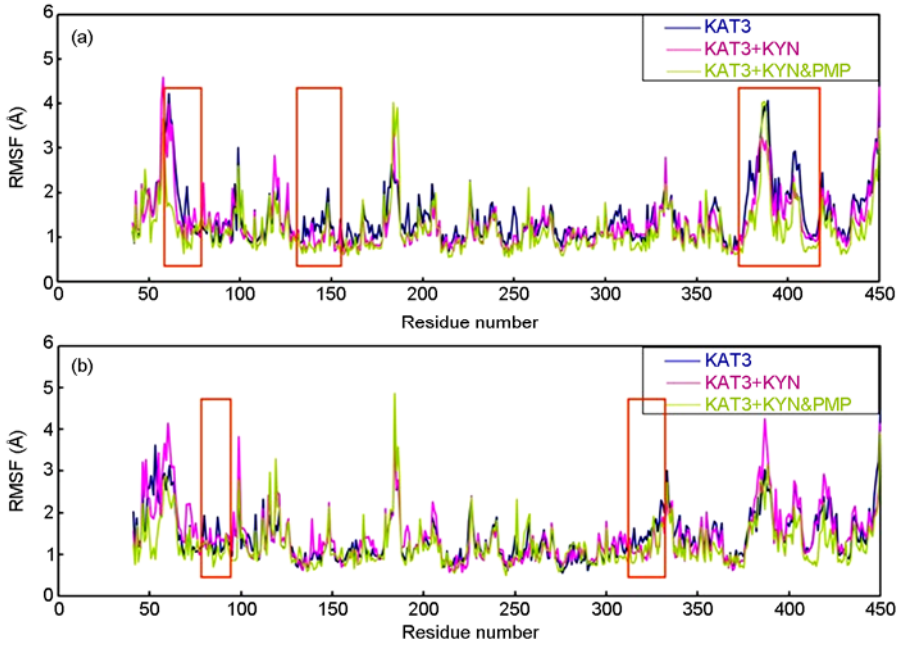

Figure 4 RMSF of HKAT3 and its complexes during 5 ns MD simulation, including HKAT3 alone (colored in dark blue), HKAT3&KYN complex (colored in magenta), and HKAT3&KYN&PMP complex (colored in green). The residues of the binding region are labeled. (a) chain A; (b) chain B.

tein and ligands during each of the MD simulations (Figure 5). These distances are almost the same at the beginning of MD simulation, since each of the systems is obtained from the same structure of HKAT3, while individual distances of the three systems show different types of phenomena during the MD simulations.

In the single HKAT3 system, the distance between Tyr159 and Lys280 increases from the beginning of MD run, and changes significantly around 0.6 nm in the whole MD trajectory. Since there is no ligand in single HKAT3 system, the binding pocket becomes open state to allow ligands moving in. Meanwhile, the system loses the hydrophobic interaction between Tyr159 and Lys280, which causes the increasing of the distance between these two residues. The positions of these two residues may change significantly with the high fluctuations of the binding site.

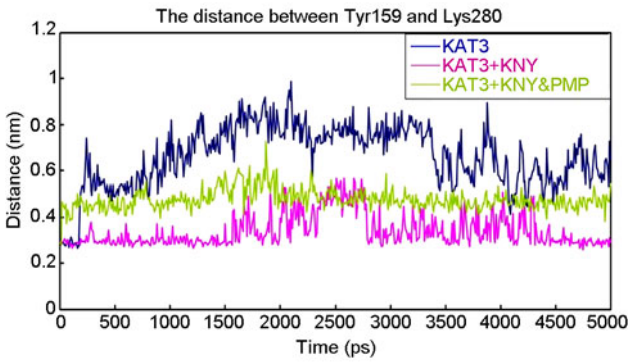

Figure 5 Distances between the O_H atom of Tyr159 and the C_Z atom of Lys280 during 5 ns MD run in each of the three systems, including HKAT3 alone (colored in dark blue), HKAT3&KYN complex (colored in magenta), and HKAT3&KYN&PMP complex (colored in green), respectively.

In the MD simulation of KYN complex, the distance is stable around 0.3 nm during the first 1.5 ns MD run. The curve of distance shows little fluctuations from 1.5 to 4.5 ns, and finally stays stable around 0.3 nm. When KYN binds to HKAT3, Tyr159 forms hydrophobic interaction with Lys280, and keeps their distance in 0.3 nm. These two residues behave as switches, and turn to close with the binding of KYN. This action prevents the ligand from moving into the binding region of the cofactor. Then the changes of distance come from the moving of benzyl moiety in Tyr135 towards Tyr159, and a hydrophobic interaction is formed between these two residues. This interaction interrupts the connection between Tyr159 and Lys280. Finally, Asn218 participates in the hydrogen-bonding network involving Tyr159 and Lys280, and it helps to stabilize the interaction network in the last 0.5 ns.

In the case of KYN&PMP complex, the distance between Tyr159 and Lys280 increases quickly, and becomes stable around 0.42 nm in the entire 5 ns MD simulation. The switches become open to allow the cofactor binding into the correct region. Tyr159 and Lys280 form an interaction network with the cofactor and the KYN, and preserve the positions of the ligands. We also measured the distance between Tyr160 and Lys281 in mouse KYN&PMP complex structure (PDB: 3E2Z), and the hydrophobic interaction between these two residues was found. However, the average value is 0.72 nm in mouse complex structure and is much higher than that in the human structure [23]. The difference of this distance between human and mouse KAT3 may indicate

that the HKAT3 may have high binding ability and high selectivity. These results may help to explain the differences of inhibitions between human and mouse KATs [48].

In summary, Tyr159 and Lys280, which form the strong hydrophobic interaction in our results, act as the switches inside the active site. This interaction may influence the binding mode and the binding region of ligands.

4.3 Effect of PMP binding

It has been reported that all the KAT enzymes have similar binding sites for the cofactor. We analyzed the sequences of some members of the KAT family to identify the key residues of cofactor binding by using ClustalW web server (Figure 6) [49]. In the case of HKAT3, based on our study, PMP is positioned correctly by forming a salt-bridge with Asp246 (Figure 7(a)). In addition, the cofactor is perfectly nested in a pocket including Tyr135, Tyr159, Cys161, Ser277 and Lys288.

On the other hand, the presence of cofactors may influence the binding of ligands. Although KYN moieties of both complexes are located in the similar positions at the beginning of the MD simulation, individual moieties bind in completely different positions in the end, and the cofactor of PMP binds in the active site stably. We superimposed the complexes of KYN and KYN&PMP (Figure 7(b)). In both systems, the aromatic ring of the KYN lies in almost the same plane and forms π-π interaction with Tyr97(B) at the beginning of the MD run (Figure 7(c)). During the MD simulation, there are two types of movements in the system without PMP: first, the aromatic ring of KYN moves towards Try311(B) by a distance of 6.47 Å; meanwhile, the indole side chain of Trp53 turns to KYN and Try311(B); finally, the aromatic ring of KYN is sandwiched by Trp53

```
HKAT3      MFLAQRSLCSLSGRAKFLKTISSS-KILGFSTSAKMSLKFTNAKRIEGLDSNVWIEFTKL 59
MKAT3      MLLAQRRLISLGCRSKPIKTIYSSSKVLGLCTSAKMALKFKNAKRIEGLDSNVWVEFTKL 60
HKAT1      ------------------------------------MAKQLQ-ARRLDGIDYNPWVEFVKL 24
HKAT2      ------------------------MNYARFITAASAARNPSPIRTMTDILSRGPKSMISL 36

HKAT3      AADPSVVNLGQGFPDISPPTYVKEELSKIAAIDS-LNQYTRGFGHPSLVKALSYLYEKLY 118
MKAT3      AADPSVVNLGQGFPDISPPSYVKEELSKAAFIDN-MNQYTRGFGHPALVKALSCLYGKIY 119
HKAT1      ASEHDVVNLGQGFPDFPPPDFAVEAFQHAVSGDFMLNQYTKTFGYPPLTKILASFFGELL 84
HKAT2      AGGLPNPNMFP-FKTAVITVENGKTIQFGEEMMKRALQYSPSAGIPELLSWLKQLQIKLH 95

HKAT3      QK------QIDSNKEILVTVGAYGSLFNTIQALIDEGDEVILIVPFYDCYEPMVRMAGAT 172
MKAT3      QR------QIDPNEEILVAVGAYGSLFNSIQGLVDPGDEVIIMVPFYDCYEPMVRMAGAV 173
HKAT1      GQ------EIDPLRNVLVTVGGYGALFTAFQALVDEGDEVIIIEPFFDCYEPMTMMAGGR 138
HKAT2      NPPTIHYPPSQGQMDLCVTSGSQQGLCKVFEMIINPGDNVLLDEPAYSGTLQSLHPLGCN 155

HKAT3      PVFIPLR-SKPV-YGKRWSSSDWTLDPQELESKFNSKTKAIILNTPHNPLGKVYNREELQ 230
MKAT3      PVFIPLR-SKPT-DGMKWTSSDWTFDPRELESKFSSKTKAIILNTPHNPLGKVYTRQELQ 231
HKAT1      PVFVSLK-PGPIQNGELGSSSNWQLDPMELAGKFTSRTKALVLNTPNNPLGKVFSREELE 197
HKAT2      IINVASDESGIVPDSLRDILSRWKPEDAKNPQKNTPKFLYTVPNG-NNPTGNSLTSERKK 214

HKAT3      VIADLCIKYDTLCISDEVYEWLVYSGNKHLKIATFPGMWERTITIGSAGKTFSVTGWKLG 290
MKAT3      VIADLCVKHDTLCISDEVYEWLVYTGHTHVKIATLPGMWERTITIGSAGKTFSVTGWKLG 291
HKAT1      LVASLCQQHDVVCITDEVYQWMVYDGHQHISIASLPGMWERTLTIGSAGKTFSATGWKVG 257
HKAT2      EIYELARKYDFLIIEDDPYYFLQFNKFRVPTFLSMD-VDGRVIRADSFSKIISS-GLRIG 272

HKAT3      WSIGPNHLIKHLQTVQQNTIYTCATPLQEALAQAFWID-----IKRMDDPECYFNSLPKE 345
MKAT3      WSIGPAHLIKHLQTVQQNSFYTCATPLQAALAEAFWID-----IKRMDDPECYFNSLPKE 346
HKAT1      WVLGPDHIMKHLRTVHQNSVFHCPTQSQAAVAESFERE-----QLLFRQPSSYFVQFPQA 312
HKAT2      FLTGPKPLIERVILHIQVSTLHPSTFNQLMISQLLHEWGEEGFMAHVDRVIDFYSNQKDA 332

HKAT3      LEVKRDRMVRLLESVGLKPIVPDGGYFIIADVSLLDPDLSDMK--NNEPYDYKFVKWMTK 403
MKAT3      LEVKRDRMVRLLNSVGLKPIVPDGGYFIIADVSSLGADLSDMN--SDEPYDYKFVKWMTK 404
HKAT1      MQRCRDHMIRSLQSVGLKPIIPQGSYFLITDISDFKRKMPDLPGAVDEPYDRRFVKWMIK 372
HKAT2      ILAAADKWLTGLAEW----HVPAAGMFLWIKVKGIN----DVK---------ELIEEKAV 375

HKAT3      HKKLSAIPVSAFCNSETKSQFEKFVRFCFIKKDSTLDAAEEIIKAWSVQKS 454
MKAT3      HKKLTAIPVSAFCDSKSKPHFEKLVRFCFIKKDSTLDAAEEIFRAWNSQKS 455
HKAT1      NKGLVAIPVSIFYSVPHQKHFDHYIRFCFVKDEATLQAMDEKLRKWKVEL- 422
HKAT2      KMGVLMLPGNAFYVDSSAPSPYLRASFSSASPEQMDVAFQVLAQLIKESL- 425
```

Figure 6 Multiple sequence alignment of KAT I (KAT1), KAT II (KAT2) and KAT III (KAT3), which are conserved in KATs found in humans (HKAT3) and KAT3 found in mice (MKAT3). The key residues are labeled.

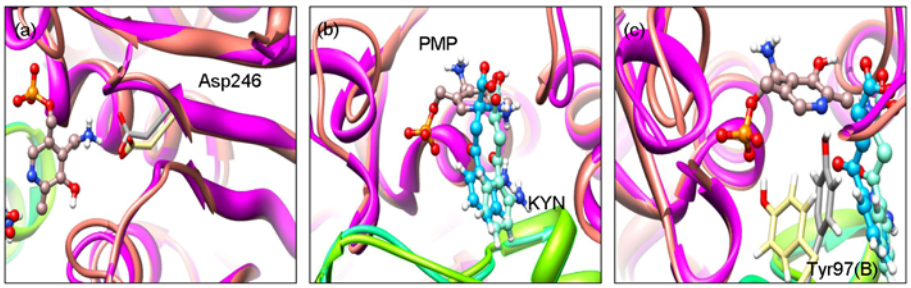

Figure 7 Superposition of structures at the beginning of the MD simulation. The snapshots of three systems during 5 ns MD run. The system of HKAT3&KYN complex: chain A is in salmon, chain B is in spring green and the ligand is shown in ball & stick (KYN in turquoise). The system of HKAT3&KYN&PMP complex: chain A is in magenta, chain B is in chartreuse and the ligands are shown in ball & stick (KYN in cyan and PMP in rosy brown). (a) Ligands; (b) Asp246; (c) Tyr97(B).

and Try311(B) *via* π-π interaction (Figure 8). Upon the presence of PMP, however, the position of KYN is highly conserved. With the presence of PMP, the fraction of hydrophobic interaction increases from 0.17 to 0.52 in position 312, and fraction of Lys280 increases from 0.06 to 0.45 during MD simulation. Moreover, the fraction of hydrogen binding interaction is also influenced by PMP, such as Gly71 (0.23 to 0.43) and Arg429 (0.19 to 0.73). The total fraction of hydrophobic interactions and hydrogen-bonding interactions between KYN and HKAT3 increases from 4.41 to 6.14 and from 2.51 to 3.23, respectively (Tables 1 and 2). Moreover, the C_α RMSD calculating between the average structures in both complex systems was 0.17 nm. The result shows that the presence of PMP may influence the biological structure of human HKAT3, especially the binding region. The average interaction energy between HKAT3 and KYN for in the absence and presence of PMP is −7.66 kcal/mol and −9.51 kcal/mol, respectively. The results mentioned above indicate that the PMP increases the ability of KYN binding. Since a better binding mode gives lower energy, we conjecture that PMP is important not only to the catalysis, but also to the binding interaction with other ligands.

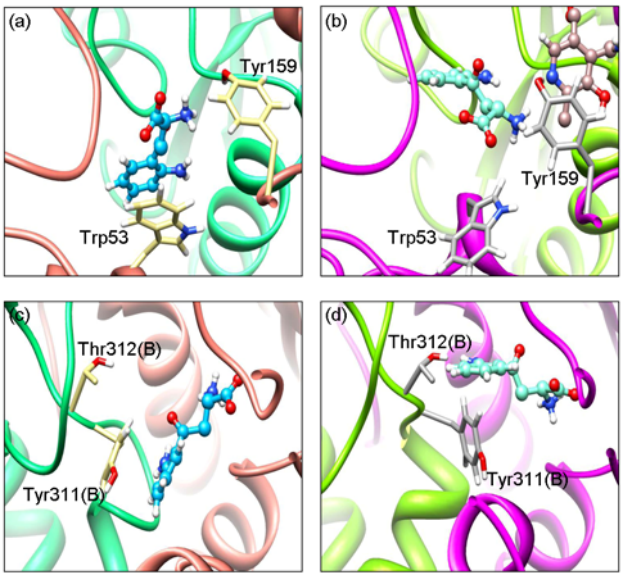

Figure 8 Interaction between the protein and ligands. The system of HKAT3&KYN complex: chain A is in salmon, chain B is in spring green and the ligand is shown in ball & stick (KYN in turquoise). The system of HKAT3&KYN&PMP complex: chain A is in magenta, chain B is in chartreuse and the ligands are shown in ball & stick (KYN in cyan and PMP in rosy brown). (a) The ligand interacts with Trp13 and Tyr159 in HKAT3&KYN complex; (b) the ligands interact with Trp13 and Tyr159 in HKAT3&KYN&PMP complex; (c) the ligand interacts with Tyr311(B) and Thr312(B) in HKAT3&KYN complex; (d) the ligands interact with Tyr311(B) and Thr312(B) in HKAT3&KYN&PMP complex.

5 Conclusion

In this study, we focus on the action of HKAT3 involved in the KYN pathway, especially the structure-function relationship among KYN, PMP and the protein. With the published homology model of HKAT3, the binding models of KYN complex and KYN&PMP complex were obtained and were studied by molecular dynamic (MD) simulations. These binding modes of the complexes are in satisfactory agreement with known experimental data. Based on these results, we arrive at the following conclusions:

(1) Several critical residues (Trp53, Try97(B), Arg246, Try311(B), Arg429) are identified in both systems for ligand binding using the residue-based decomposition.

(2) The conformational changes of HKAT3 may allow the recognition of ligands and will plug the active center after binding.

(3) Tyr159 and Lys280, which form strong hydrophobic interaction based on our results, act as the switches inside the active site. This interaction may influence the binding mode and the binding region of the substrate and the cofactor.

(4) In the transformation of KYNA, the PMP contribute largely not only to the catalysis, but also to the binding

Our study offers a stepwise conformational analysis, which leads to a thorough and fruitful investigation of favored adopting conformers in solution. The results of this study are not limited within HKAT3, and they can also be extended to other members of KAT family. Thus, the ap-

plied strategy may expand the scope of drug design.

This work was financially supported by the National Natural Science Foundation of China, Specialized Research Fund for the Doctoral Program of Higher Education, and Specialized Fund for the Basic Research of Jilin University (20903045, 20573042, 20070183046,200810018).

1 Hilmas C, Pereira EF, Alkondon M, Rassoulpour A, Schwarcz R, Albuquerque EX. The brain metabolite kynurenic acid inhibits α7 nicotinic receptor activity and increases non-α7 nicotinic receptor expression: Physiopathological implications. *J Neurosci*, 2001, 21: 7463–7473
2 Alkondon M, Pereira EF, Yu P, Arruda EZ, Almeida LE, Guidetti P, Fawcett WP, Sapko MT, Randall WR, Schwarcz R, Tagle DA, Albuquerque EX. Targeted deletion of the kynurenine aminotransferase ii Gene reveals a critical role of endogenous kynurenic acid in the regulation of synaptic transmission *via* α7 nicotinic receptors in the hippocampus. *J Neurosci*, 2004, 24: 4635–4648
3 Stone TW. Kynurenic acid blocks nicotinic synaptic transmission to hippocampal interneurons in young rats. *Eur J Neurosci*, 2007, 25: 2656–2665
4 Wang J, Simonavicius N, Wu X, Swaminath G, Reagan J, Tian H, Ling L. Kynurenic acid as a ligand for orphan G protein-coupled receptor GPR35. *J Biol Chem*, 2006, 281: 22021–22028
5 Leeson PD, Iversen LL. The glycine site on the NMDA receptor: Structure-activity relationships and therapeutic potential. *J Med Chem*, 1994, 37: 4053–4067
6 Perkins MN, Stone TW. An iontophoretic investigation of the actions of convulsant kynurenines and their interaction with the endogenous excitant quinolinic acid. *Brain Res*, 1982, 247: 184–187
7 Stone TW, Perkins MN. Actions of excitatory amino acids and kynurenic acid in the primate hippocampus: A preliminary study. *Neurosci Lett*, 1984, 52: 335–340
8 Birch PJ, Grossman CJ, Hayes AG. Kynurenic acid antagonizes responses to NMDA *via* an action at the strychnine-insensitive glycine receptor. *Eur J Pharmacol*, 1988, 154: 85–87
9 Pereira EF, Hilmas C, Santos MD, Alkondon M, Maelicke A, Albuquerque EX. Unconventional ligands and modulators of nicotinic receptors. *J Neurobiol*, 2002, 53: 479–500
10 Beal MF, Matson WR, Swartz KJ, Gamache PH, Bird ED. Kynurenine pathway measurements in Huntington's disease striatum: Evidence for reduced formation of kynurenic acid. *J Neurochem*, 1990, 55: 1327–1339
11 Guidetti P, Reddy PH, Tagle DA, Schwarcz R. Early kynurenergic impairment in Huntington's disease and in a transgenic animal model. *Neurosci Lett*, 2000, 283: 233–235
12 Widner B, Leblhuber F, Walli J, Tilz GP, Demel U, Fuchs D. Tryptophan degradation and immune activation in Alzheimer's disease. *J Neural Transm*, 2000, 107: 343–353
13 Erhardt S, Blennow K, Nordin C, Skogh E, Lindstrom LH, Engberg G. Kynurenic acid levels are elevated in the cerebrospinal fluid of patients with schizophrenia. *Neurosci Lett*, 2001, 313: 96–98
14 Erhardt S, Schwieler L, Nilsson L, Linderholm K, Engberg G. The kynurenic acid hypothesis of schizophrenia. *Physiol Behav*, 2007, 92: 203–209
15 Schwarcz R, Rassoulpour AA, Wu HQ, Medoff D, Tamminga CA, Roberts RC. Increased cortical kynurenate content in schizophrenia. *Biol Psychiatry*, 2001, 50: 521–530
16 Guillemin GJ, Kerr SJ, Brew BJ. Involvement of quinolinic acid in AIDS dementia complex. *Neurotox Res*, 2005, 7: 103–123
17 Guidetti P, Amori L, Sapko MT, Okuno E, Schwarcz R. Mitochondrial aspartate aminotransferase: A third kynurenate-producing enzyme in the mammalian brain. *J Neurochem*, 2007, 102: 103–111
18 Yu P, Li Z, Zhang L, Tagle DA, Cai T. Characterization of kynurenine aminotransferase III, A novel member of a phylogenetically conserved KAT family. *Gene*, 2006, 365: 111–118
19 Okuno E, Nakamura M, Schwarcz R. Two kynurenine aminotransferases in human brain. *Brain Res*, 1991, 542: 307–312
20 Guidetti P, Okuno E, Schwarcz R. Characterization of rat brain kynurenine aminotransferases I and II. *J Neurosci Res*, 1997, 50: 457–465
21 Schwarcz R, Pellicciari R. Manipulation of brain kynurenines: Glial targets, neuronal effects, and clinical opportunities. *J Pharmacol Exp Ther*, 2002, 303: 1–10
22 Han Q, Li J, Li J. pH dependence, substrate specificity and inhibition of human kynurenine aminotransferase I. *Eur J Biochem*, 2004, 271: 4804–4814
23 Han Q, Robinson H, Cai T, Tagle DA, Li J. Biochemical and structural properties of mouse kynurenine aminotransferase III. *Mol Cell Biol*, 2009, 29: 784–793
24 Goh DL, Patel A, Thomas GH, Salomons GS, Schor DS, Jakobs C, Geraghty MT. Characterization of the human gene encoding alpha-aminoadipate aminotransferase (AADAT). *Mol Genet Metab*, 2002, 76: 172–180
25 Martini F, Angelaccio S, Barra D, Pascarella S, Maras B, Doonan S, Bossa F. The primary structure of mitochondrial aspartate aminotransferase from human heart. *Biochim Biophys Acta*, 1985, 832: 46–51
26 Papadimitriou JM, Duijn P. The ultrastructural localization of the isozymes of aspartate aminotransferase in murine tissues. *J Cell Biol*, 1970, 47: 84–98
27 Tanaka M, Takeda N, Tohyama M, Matsunaga T. Immunocytochemical localization of mitochondrial and cytosolic aspartate aminotransferase isozymes in the vestibular endorgans of rats. *Eur Arch Otorhinolaryngol*, 1990, 247: 119–121
28 Giannattasio S, Marra E, Abruzzese MF, Greco M, Quagliariello E. The in vitro-synthesized precursor and mature mitochondrial aspartate aminotransferase share the same import pathway in isolated mitochondria. *Arch Biochem Biophys*, 1991, 290: 528–534
29 Faff-Michalak L, Albrecht J. Aspartate aminotransferase, malate dehydrogenase, and pyruvate carboxylase activities in rat cerebral synaptic and nonsynaptic mitochondria: Effects of *in vitro* treatment with ammonia, hyperammonemia and hepatic encephalopathy. *Metab Brain Dis*, 1991, 6: 187–197
30 McKenna MC, Stevenson JH, Huang X, Hopkins IB. Differential distribution of the enzymes glutamate dehydrogenase and aspartate aminotransferase in cortical synaptic mitochondria contributes to metabolic compartmentation in cortical synaptic terminals. *Neurochem Int*, 2000, 37: 229–241
31 Cechetto JD, Sadacharan SK, Berk PD, Gupta RS. Immunogold localization of mitochondrial aspartate aminotransferase in mitochondria and on the cell surface in normal rat tissues. *Histol Histopathol*, 2002, 17: 353–364
32 Shrawder E, Martinez-Carrion M. Evidence of phenylalanine transaminase activity in the isoenzymes of aspartate transaminase. *J Biol Chem*, 1972, 247: 2486–2492
33 Suzuki T, Kishi Y, Totani M, Kagamiyama H, Murachi T. Monoclonal and polyclonal antibodies against porcine mitochondrial aspartate aminotransferase: Their inhibition modes and application to enzyme immunoassay. *Biotechnol Appl Biochem*, 1987, 9: 170–180
34 Mawal MR, Mukhopadhyay A, Deshmukh DR. Purification and properties of alpha-aminoadipate aminotransferase from rat liver and kidney mitochondria. *Prep Biochem*, 1991, 21: 151–162
35 Takeuchi F, Otsuka H, Shibata Y. Purification, characterization and identification of rat liver mitochondrial kynurenine aminotransferase with α-aminoadipate aminotransferase. *Biochim Biophys Acta*, 1983, 743: 323–330
36 Rossi F, Han Q, Li J, Li J, Rizzi M. Crystal structure of human kynurenine aminotransferase I. *J Biol Chem*, 2004, 279: 50214–50220
37 Xu Y, Zheng Q C, Zhang H X, Sun CC. Homology modeling and substrate binding study of human kynurenine aminotransferase III. *J Theor Comput Chem*, 2012, 11(4): 855–870
38 Hess B, Kutzner C, van der Spoel D, Lindahl E. GROMACS 4: Algorithms for highly efficient, load-balanced, and scalable molecular simulation. *J Chem Theory Comput*, 2008, 4(3): 435–447

39 Oostenbrink C, Villa A, Mark AE, Gunsteren WF. A biomolecular force field based on the free enthalpy of hydration and solvation: The GROMOS force-field parameter sets 53A5 and 53A6. *J Comput Chem*, 2004, 25(13): 1656–1676

40 http://davapc1.bioch.dundee.ac.uk/prodrg/

41 Darden T, York D, Pedersen L. Particle mesh Ewald: An $N\cdot\log(N)$ method for Ewald sums in large systems. *J Chem Phys*, 1993, 98: 10089–10092

42 Essmann U, Perera L, Berkowitz M L. A smooth particle mesh Ewald method. *J Chem Phys*, 1995, 103: 8577–8593

43 Hess B, Bekker H, Berendsen HJC, Fraaije JGEM. LINCS: A linear constraint solver for molecular simulations. *J Comput Chem*, 1997, 18: 1463–1472

44 Humphrey W, Dalke A, Schulten K. VMD: Visual molecular dynamics. *J Mol Graph*, 1996, 14(1): 33–8, 27–8

45 Eric F. Pettersen, Thomas D. Goddard, Conrad C. Huang, Gregory S. Couch, Daniel M. Greenblatt, Elaine C. Meng, Thomas E. Ferrin. UCSF Chimera—A visualization system for exploratory research and analysis. *J Comput Chem*, 2004, 25(13): 1605–1612

46 Mezei M. Simulaid: A simulation facilitator and analysis program. *J Comput Chem*, 2010, 31(14): 2658–2668

47 Hu JP, Chang C, Chen WZ. Study on the drug resistance and the binding mode of HIV-1 integrase with LCA inhibitor. *Sci China Ser B*, 2007, 50(5): 665–674

48 Han Q, Cai T, Tagle DA, Li JY. Structure, expression, and function of kynurenine aminotransferases in human and rodent brains. *Cell Mol Life Sci*, 2010, 67: 353–368

49 http://www.ebi.ac.uk/Tools/msa/clustalw2/

SCIENCE CHINA
Chemistry

• SUPPORTING INFORMATION •

April 2013 Vol.56 No.4: 1–2
doi: 10.1007/s11426-012-4802-8

A molecular dynamics and computational study of human KAT3 involved in KYN pathway

XU Yu, ZHENG QingChuan*, YU LiYing, ZHANG HongXing* & SUN ChiaChung

State Key Laboratory of Theoretical and Computational Chemistry, Institute of Theoretical Chemistry, Jilin University, Changchun 130023, China

Received August 3, 2012; accepted August 20, 2012; published online December 31, 2012

1 Monomer homology modeling and MD simulation

The primary sequence of HKAT3 was obtained from the SwissProt database (accession number Q6YP21). The X-ray crystal structure of mouse KAT3 was taken from the Protein Data Bank (PDB code 3E2Y) [23]. Since the N-terminus domain (aa1-40) is away from the active site of HKAT3 and the counterpart of the template protein is missing, this part was not used to built the model. The homology modeling was performed in two steps. First, the template was used to create three different models of HKAT3. The Num_Loop_Models was set to 1 to reduce the computational time. The best monomer model was evaluated by their stereochemical quality with the program of DS and was selected to refine. Then the initial model was subjected to MD simulation to refine the model.

2 Results

2.1 Homology models construction and evaluation

Final model of HKAT3 monomer was assessed by Profile-3D and Procheck. By Profile-3D, a Verify Score vs. Amino Acid was displayed in Figure S1(a). It is not surprising that most of the amino acids are in favored regions, and the residues, with the verify score less than zero, were allowed corresponding to loop region and template. The reliability backbone torsion angles Φ-ψ of the target proteins were examined by Procheck, and the template was also evaluated for comparison. The percentage of Φ-ψ angles in allowed Ramachandran region is 99% in the HKAT3 monomer model. From the statistical score of the Ramachandran plot Fig. S1b, we could see among the 410 residues 94.1% are in the most favored regions. Above all, the results of quality assessment suggest that the model of HKAT3 monomer structure is reliable.

*Corresponding authors (email: zhengqc@jlu.edu.cn; zhanghx@jlu.edu.cn)

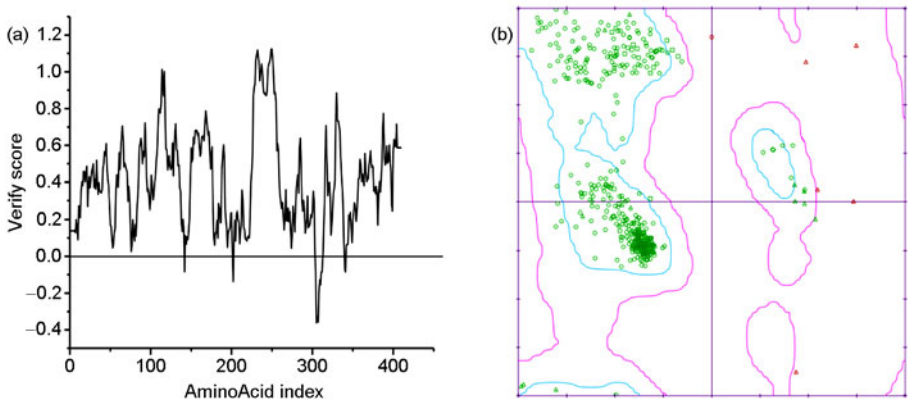

Figure S1 The results of HKAT3 model. (a) The 3D-verify analysis of HKAT3 model; (b) Ramachandran plot of HKAT3 model.

2.2 Schematic structures of KYN and PMP

The schematic structures of KYN and PMP were obtained by using ChemDraw (in Figure S2).

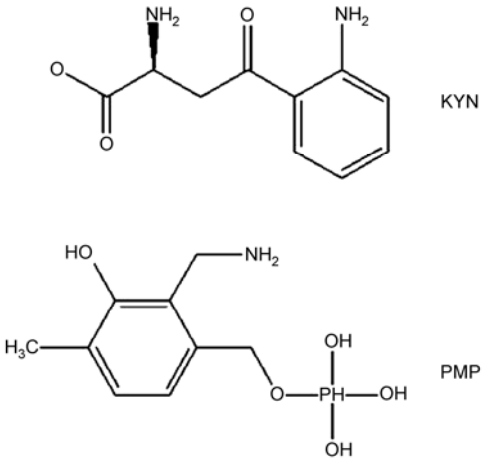

Figure S2 The schematic structures of kynurenine (KYN) and pyridoxamine 5-phosphate (PMP).